Supplementary Information:

Gate Tunable Cooperativity between Vibrational Modes

*Parmeshwar Prasad, Nishta Arora, and A. K. Naik**

Indian Institute of Science, Bangalore, India, 560012

I. Fabrication method and measurement technique:

We use sapphire substrate for fabrication of the device to reduce parasitic capacitance. Low parasitic capacitance allows us to use homodyne electrical measurement technique. Homodyne electrical measurement scheme offers a simpler set-up and is faster technique compared to the other techniques such as heterodyne frequency mixdown and frequency modulation technique.[1] To fabricate the device, a metal gate Ti/Pt (15/10 nm) is deposited on the substrate using thermal deposition. Next, 300 nm thick SiO_2 is deposited using plasma enhanced chemical vapor deposition (PECVD). A circular window is exposed, covering the remaining SiO_2 with Cr mask. The circular trench is obtained by etching the exposed SiO_2 using reactive ion etching (RIE). For the source-drain metal contact pads, Cr/Au (5/50 nm) is deposited a few μm away from the trench. To suspend MoS_2 membrane, a PDMS sheet with exfoliated MoS_2 flake is placed on top of the circular trench and the flake is transferred over it such that the membrane also makes contacts with source-drain pads.[2]

We perform the measurements using capacitive actuation and detection technique. We use an AC signal source V_g^{ac} which is combined with a DC voltage V_g^{dc} using a bias tee. This combined AC and DC signal is applied at the gate. The oscillating force actuates the resonator and hence changes the capacitance between the membrane and the gate. The output signal at the drain is given by the following equation[3]:

$$\frac{\tilde{V}}{R} = i\omega_d C_p V_g^{ac} - i\omega_d \frac{\tilde{z}}{z_0} C_g V_g^{dc} \quad \text{(S1)}$$

Where $\tilde{V}$ is the output voltage, R input impedance of the amplifier, C_p is the parasitic capacitance, C_g is the capacitance between the membrane and the gate separated by a distance z_0. First term in the equation is the electrical background which can be estimated by setting $V_g^{dc} = 0$. The second term is because of the displacement of the membrane ($\tilde{z}$).

To perform red and blue-detuned pumping, another AC signal source is combined with drive signal using an RF combiner.

II. **Theoretical model:**

The simulations are performed in Wolfram Mathematica 9.0 using the equation of motion for coupled resonators in the following way[4]:

$$\ddot{X}_l + \gamma_l \dot{X}_l + \left[\Omega_l^2 + \alpha_l F_{lp}(t)\right] X_l = k_c(X_h - X_l) + F_l(t) \#(S2)$$

$$\ddot{X}_h + \gamma_h \dot{X}_h + \left[\Omega_h^2 + \alpha_h F_{lp}(t)\right] X_2 = k_c(X_l - X_h) + F_h(t) \#(S3)$$

Where subscript l and h denote the lower and higher mode numbers. Ω_l and Ω_h are eigenfrequencies of the modes, $\Omega_h = \Omega_l + \delta\Omega$. We assume $\gamma_l = \gamma_h = \gamma$ for simplifying the equations. The softening parameters $\alpha(l,h)$ are due to change in membrane tension with applied DC gate force .ie. $\alpha \propto \frac{\partial T}{\partial F}$. The softening parameters are mode dependent. In our experiments the applied parametric force $F_{lp}(t) = F_{hp}(t) = F_p = \frac{\partial C_g}{\partial x} V_g^{dc} V_p^{ac} \cos(\omega_p t)$ and $F_l(t) = F = \frac{\partial C_g}{\partial x} V_g^{dc} V_g^{ac} \cos(\omega_d t)$ and $F_h(t) = 0$. The equations S2 and S3 can be written in the following way:

$$\ddot{X}_l + \gamma \dot{X}_l + \left[\Omega_l^2 + \alpha_l F_p\right] X_l = k_c (X_h - X_l) + F \#(S4)$$

$$\ddot{X}_h + \gamma \dot{X}_h + \left[\Omega_l^2 + 2\Omega_l \delta\Omega + \delta\Omega^2 + \alpha_h F_p\right] X_h = k_c (X_l - X_h) \#(S5)$$

$$\left[\frac{d}{dt^2} + \gamma \frac{d}{dt} + \Omega_l^2 + k_c + \Omega_l \delta\Omega + \frac{\delta\Omega^2}{2}\right] \begin{bmatrix} X_l \\ X_h \end{bmatrix} - \begin{bmatrix} \left(\Omega_l \delta\Omega + \frac{\delta\Omega^2}{2}\right) & k_c \\ k_c & -\left(\Omega_l \delta\Omega + \frac{\delta\Omega^2}{2}\right) \end{bmatrix} \begin{bmatrix} X_l \\ X_h \end{bmatrix} + \begin{bmatrix} \alpha_l F_p & 0 \\ 0 & \alpha_h F_p \end{bmatrix} \begin{bmatrix} X_l \\ X_h \end{bmatrix} = \begin{bmatrix} F \\ 0 \end{bmatrix} \#(S6)$$

Using the diagonalization matrix $U = \frac{1}{2\lambda} \begin{bmatrix} \sqrt{\lambda + \zeta} & \sqrt{\lambda - \zeta} \\ \sqrt{\lambda - \zeta} & \sqrt{\lambda + \zeta} \end{bmatrix}$, where $\lambda = \sqrt{\left(\Omega_l \delta\Omega + \frac{\delta\Omega^2}{2}\right)^2 + {k_c}^2}$ and $\zeta = \Omega_l \delta\Omega + \frac{\delta\Omega^2}{2}$. The above equations of motion can be transformed using the new basis vector $\left(\begin{pmatrix} x_l \\ x_h \end{pmatrix} = U \begin{pmatrix} X_l \\ X_h \end{pmatrix}\right)$ in the following way

$$\left[\frac{d}{dt^2}+\gamma\frac{d}{dt}+\Omega_l^2+k_c+\Omega_l\delta\Omega+\frac{\delta\Omega^2}{2}\right]\begin{bmatrix}x_l\\x_h\end{bmatrix}-\begin{bmatrix}\lambda & 0\\0 & -\lambda\end{bmatrix}\begin{bmatrix}x_l\\x_h\end{bmatrix}$$
$$+U.\begin{bmatrix}\alpha_l F_p & 0\\0 & \alpha_h F_p\end{bmatrix}.U.\begin{bmatrix}x_l\\x_h\end{bmatrix}=U.\begin{bmatrix}F\\0\end{bmatrix}\#(S7)$$

Re-writing equation S7 as:

$$\ddot{x_l}+\gamma_l\dot{x_l}+\left[\omega_l^2+\Gamma_l\cos(\omega_p t)\right]x_l+\Lambda\cos(\omega_p t)x_h=F_l\cos(\omega_d t+\phi) \quad \text{(S8)}$$

$$\ddot{x}_h+\gamma_h\dot{x}_h+\left[\omega_h^2+\Gamma_h\cos(\omega_p t)\right]x_h+\Lambda\cos(\omega_p t)x_l=F_h\cos(\omega_d t+\phi) \quad \text{(S9)}$$

Where x are the displacements, γ are the corresponding damping rate of the modes, Γs and Λ are the intra and inter-modal coupling coefficients respectively, ω_l and ω_h are the lower and the higher dynamical modes. ω_d is the driving frequency at which the forces F are applied on the modes. ω_p is the pumping frequency by which the coupling between two modes is manipulated. The phase between the drive and the pump is given by ϕ.

$\Gamma_{l,h}$, Λ and $\omega_{l,h}$ are given by

$$\Lambda=F_p(U_{11}U_{21}\alpha_l+U_{21}U_{22}\alpha_h)=\frac{k_c F_p(\alpha_l-\alpha_h)}{2\lambda}$$

$$\Gamma_l=F_p(\alpha_l U_{11}^2+\alpha_h U_{21}^2)=\tfrac{F_p}{2\lambda}(\alpha_l(\lambda+\zeta)+\alpha_h(\lambda-\zeta))$$

$$\Gamma_h=F_p(\alpha_l U_{21}^2+\alpha_h U_{22}^2)=\tfrac{F_p}{2\lambda}(\alpha_l(\lambda-\zeta)+\alpha_h(\lambda+\zeta))$$

$$\omega_l=\sqrt{\Omega_l^2+k_c+\Omega_l\delta\Omega+\frac{\delta\Omega^2}{2}-\lambda}$$

$$\omega_h=\sqrt{\Omega_l^2+k_c+\Omega_l\delta\Omega+\frac{\delta\Omega^2}{2}+\lambda}$$

III. Simulation details:

We use the above-mentioned coupled equations S8 and S9 to simulate the observed inter and intramode coupling between mode 2 and mode 3 in the first device (device 1).

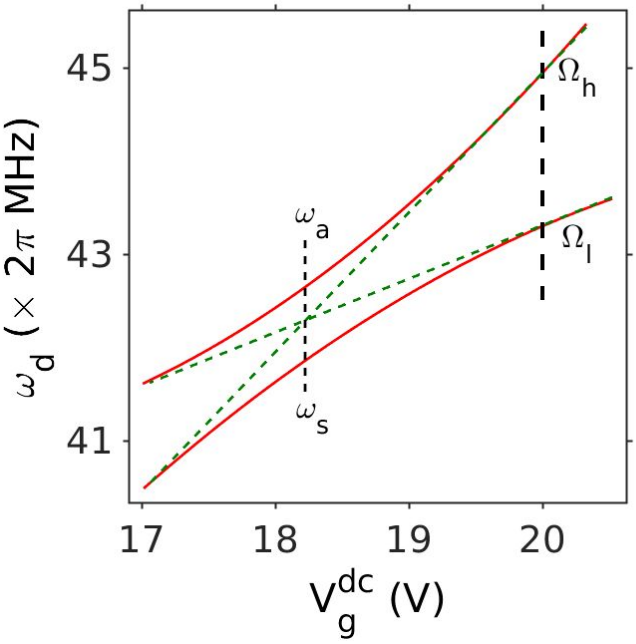

Figure S1. Avoided crossing of the two modes close to each other in device 1. The subscript l and h denotes lower and higher mode respectively. Green dotted lines are eigen frequency of the modes when the coupling is zero. The modes are tuned perfectly at $V_g^{dc} = 18.2$ V.

As shown in figure S1 Ω_l , Ω_h are $2\pi \times 43.3$ MHz and $2\pi \times 45.0$ MHz respectively at $V_g^{dc} = 20$V. Anti-Stoke ω_a and Stoke ω_s are $2\pi \times 42.6$ MHz and $2\pi \times 41.8$ MHz respectively. The coupling constant $k_c = \frac{\omega_a^2 - \omega_s^2}{2}$ along the black dotted lines at $V_g^{dc} = 18.2$ V. We define $\Gamma_0 = \frac{2\pi\omega_l^2}{Q}$, the condition for strong coupling is $\Gamma \geq \Gamma_0$. We only drive the first mode. i.e. $F_l = F$ and $F_h = 0$. For simplicity, ϕ is set to zero. In the first device (device 1), we have $\omega_l = 2\pi \times 43.2$ MHz and $\omega_h = 2\pi \times 45.0$ MHz . Damping rates $\gamma_l, \gamma_h \approx \Omega_l/Q$, where Q is the quality factor.

Equations S8 and S9 are solved numerically using rotating-frame approximation. The solution is given by the following form:

$$x_l = Re[\sum_{m=-\infty}^{m=\infty} a_m(t) e^{i(\omega + m\,\omega_p)t}]$$

$$x_h = Re[\sum_{m=-\infty}^{m=\infty} b_m(t) e^{i(\omega + m\,\omega_p)t}]$$

The equation of motion in terms of the series solution is as follows:

$$\left[-(\omega_d + m\omega_p)^2 + i\,\gamma_l(\omega_d + m\omega_p) + \omega_l^2\right]a_m + \frac{\Gamma_l}{2}(a_{m+1} + a_{m-1}) + \frac{\Lambda}{2}(b_{m+1} + b_{m-1}) = F \quad \text{(S10)}$$

$$\left[-(\omega_d + m\omega_p)^2 + i\,\gamma_h(\omega_d + m\omega_p) + \omega_h^2\right]b_m + \frac{\Gamma_h}{2}(b_{m+1} + b_{m-1}) + \frac{\Lambda}{2}(a_{m+1} + a_{m-1}) = 0 \quad \text{(S11)}$$

Here, higher order time dependent derivatives are neglected. Only the lower mode is driven with the force F and the force on the higher mode is set to zero. The simulations are performed for m = 4, and $4 \times m + 2$ equations are simultaneously solved to get the coefficients.

IV. Cooling of the mode 1 (ω_1):[5]

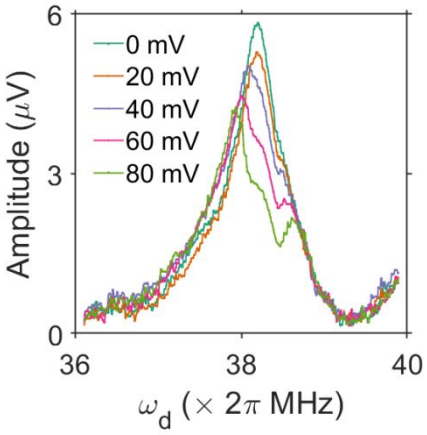
0 mV
20 mV
40 mV
60 mV
80 mV
Amplitude (μV)
6
3
0
36
38
40
ω_d (× 2π MHz)

(a)

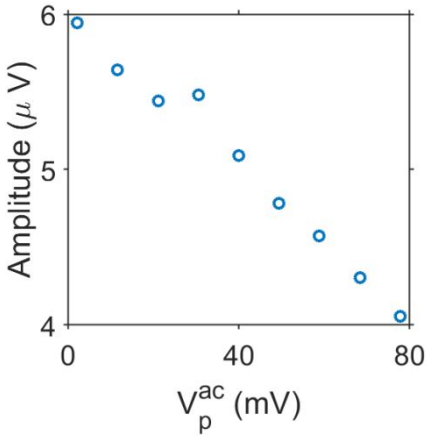
Amplitude (μ V)
6
5
4
0
40
80
V_p^ac (mV)

(b)

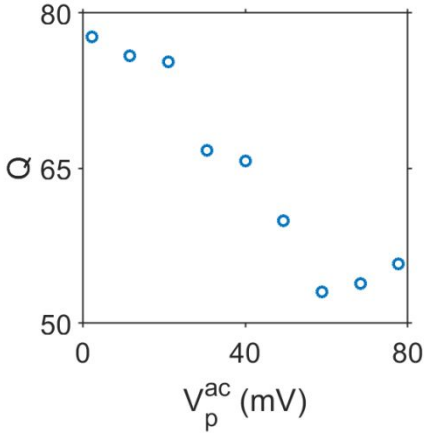
Q
80
65
50
0
40
80
V_p^ac (mV)

(c)

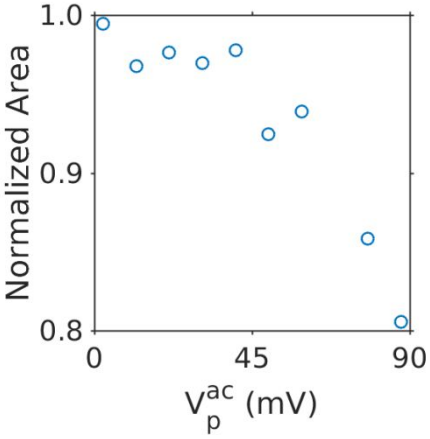
Normalized Area
1.0
0.9
0.8
0
45
90
V_p^ac (mV)

(d)

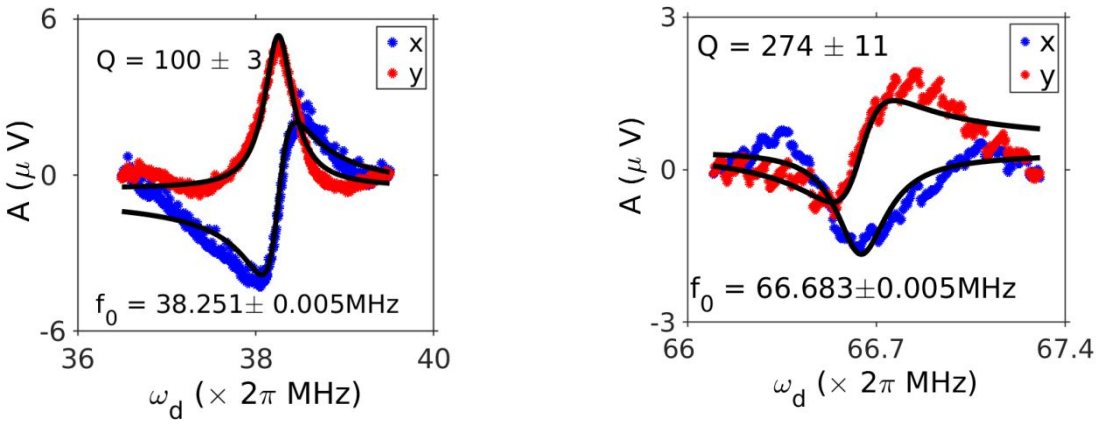

(e) (f)

Figure S2. (a) Amplitude response curve of mode 1 with V_p^{ac} for red detuned pumping. The amplitude of the response curve decreases with an increase in pump strength. The response curve splits beyond 60 mV V_p^{ac} indicating strong coupling. (b) amplitude (c) quality factor (d) normalized area under the curve vs pump strength V_p^{ac}. The decrease in area under the response curve with increase in pump strength indicates that the phonon from the mode 1 is transferred to the mode 4, resulting in cooling of mode 1. (e) and (f) are x and y quadrature of mode 1 and mode 4, lines are the fit derived using Lorentzian equation.

V. Observation of higher order splitting in device 1:

Figure S3 shows the results of red-detuned pumping between mode 1 (ω_1) and mode 4 (ω_4) in the strong coupling regime. Mode splitting at other than multiple of $\frac{\omega_p}{n}$ ($n = 1,2,3...$) are also observed. These splitting (other than marked by arrows) could not be explained by the equations S2 and S3.

We attribute these splitting to non-linear effects. The non-linear terms may contain higher order harmonics leading to mixing of those modes which appears at pump frequency other than the multiples of $\frac{\omega_p}{n}$. To confirm this attribution, further study is required.

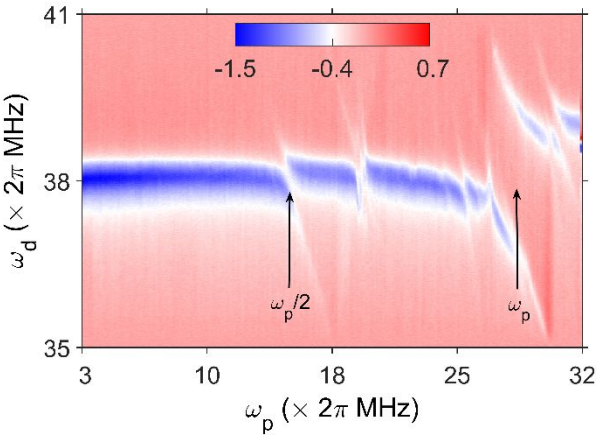

Figure S3. Inter and intra mode splitting observed around mode 1 due to coupling between the two distant modes ω_1 and ω_4 in device 1. Several splitting other than $\frac{\omega_p}{n}$ $(n = 1,2,3\ldots)$ are observed.

VI. Strong coupling in the second device (device 2):

We studied coupling in the two devices and found maximum cooperativity between the modes ~ 900. Figure S4 (a) shows the false-colored SEM image of the second device (device 2). The device dimensions are similar to the previous one (device 1) as described in the main text. In the second device, we performed experiments to ascertain the origin of large cooperativity. Figure S4b shows frequency dispersion of two modes with V_g^{dc}. The modes are separated by more than $65(\times 2\pi$ MHz). We observe, nonlinear tuning of frequency of the modes with V_g^{dc}(see figures S4 c,d).

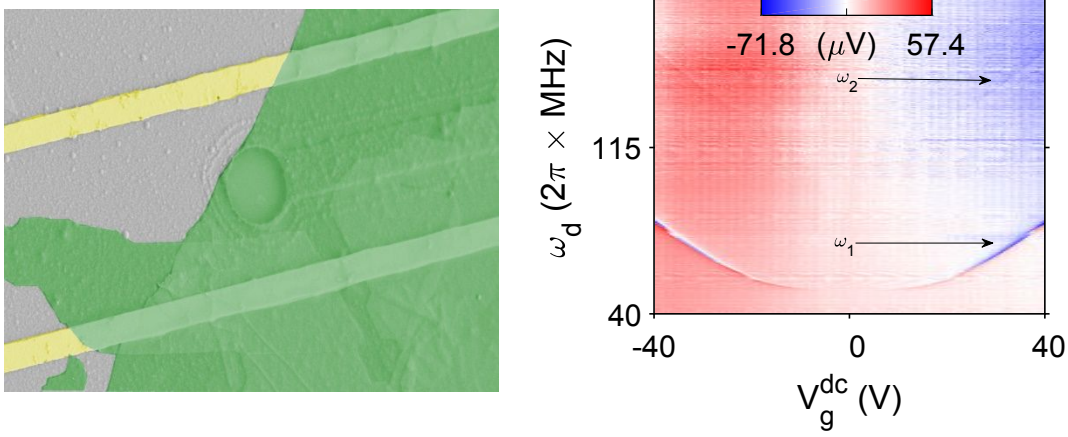

(a) (b)

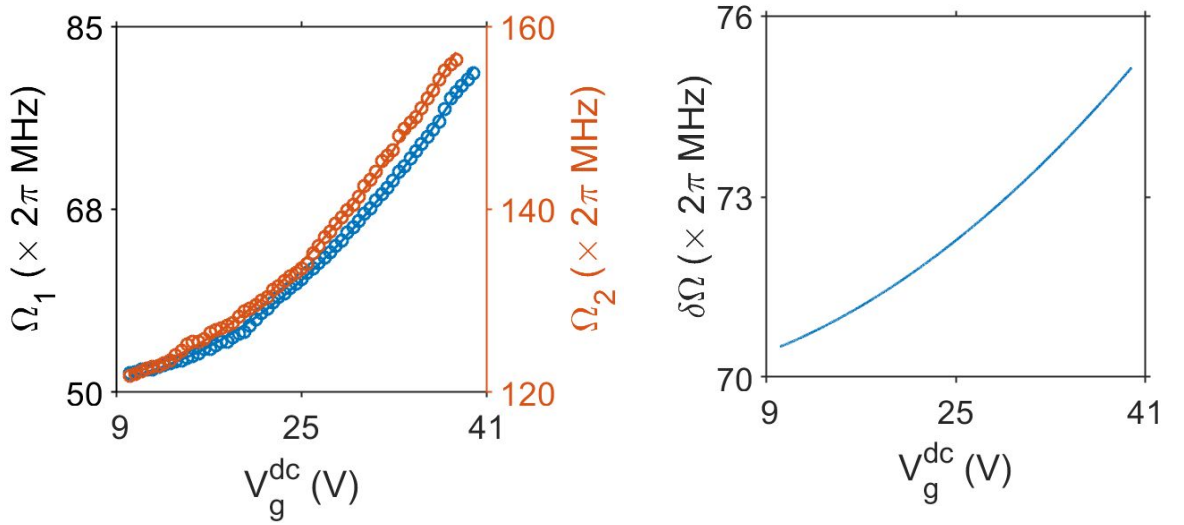

(c) (d)

Figure S4: (a) False colored scanning electron micrograph of a multilayered MoS_2 drum resonator. The drum diameter is 3 µm. (b) Frequency dispersion curve with applied gate bias V_g^{dc} . Two observed modes are seperated by more than ~ 65 MHz. (c) Comparision of the tuning of the two modes with gate voltage, The two modes have similar tuning response, however, the

subfigure (d) shows a difference of 5 MHz over the DC gate voltage of 10V to 40V range. The non-linear frequency difference indicates mode dependent frequency tuning with gate bias.

In the device 2, we performed red detuning pumping experiments on the modes at different V_g^{dc}. Figure S5 a,b show splitting of the mode in the strong coupling regime (The figures are also included in the main text). Cooperativity as high as ~ 700 has been achieved near $V_g^{dc} = 30$ V and at $V_p^{ac} = 1$ V. Beyond $V_g^{dc} = 30$ V, the tuning of the modes are such that $\Omega_p \sim \Omega_1$ posing a challenge in differentiating between pump and drive.

Figure S5c shows that the coupling rate changes linearly with the applied pump strength for different gate bias. We also observe that the slopes in the graph $\left(\frac{2g}{V_p^{ac}}\right)$ increases with applied DC gate bias (see Figure S5d), indicating the contribution of gate bias in the parametric force. Figure S5e shows the normalized slope $\left(\frac{2g}{V_p^{ac} V_g^{dc}}\right)$ with V_g^{dc}, it shows that the tuning of the tension in the membrane also contributes to increasing the coupling rate apart from parametric pump force. Based on these observations, a model of the coupling rate depending on the tuning of the modes are explained in the following section.

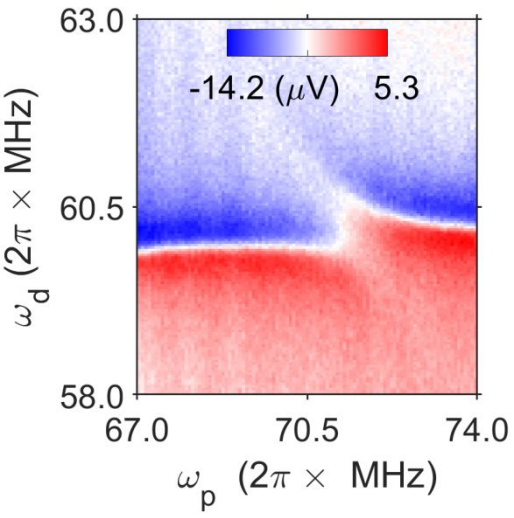
63.0
60.5
58.0
-14.2 (μV)
5.3
ω_d ($2\pi \times$ MHz)
67.0
70.5
74.0
ω_p ($2\pi \times$ MHz)

(a)

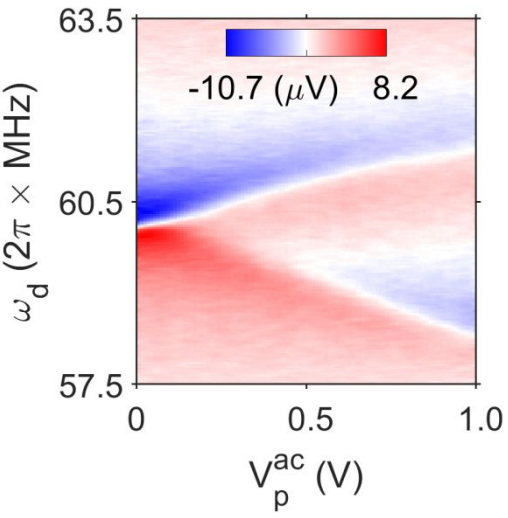
63.5
60.5
57.5
-10.7 (μV)
8.2
ω_d ($2\pi \times$ MHz)
0
0.5
1.0
V_p^{ac} (V)

(b)

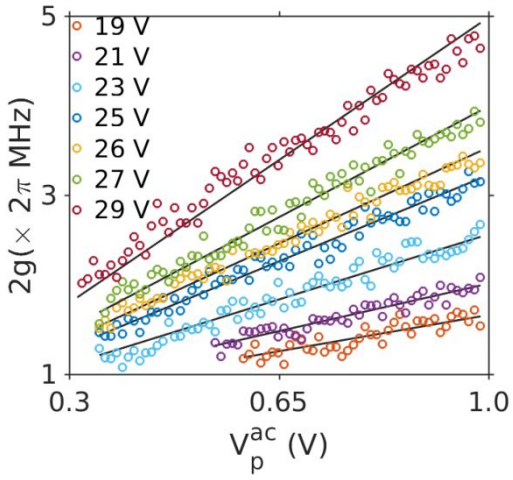
5
3
1
19 V
21 V
23 V
25 V
26 V
27 V
29 V
2g($\times 2\pi$ MHz)
0.3
0.65
1.0
V_p^{ac} (V)

(c)

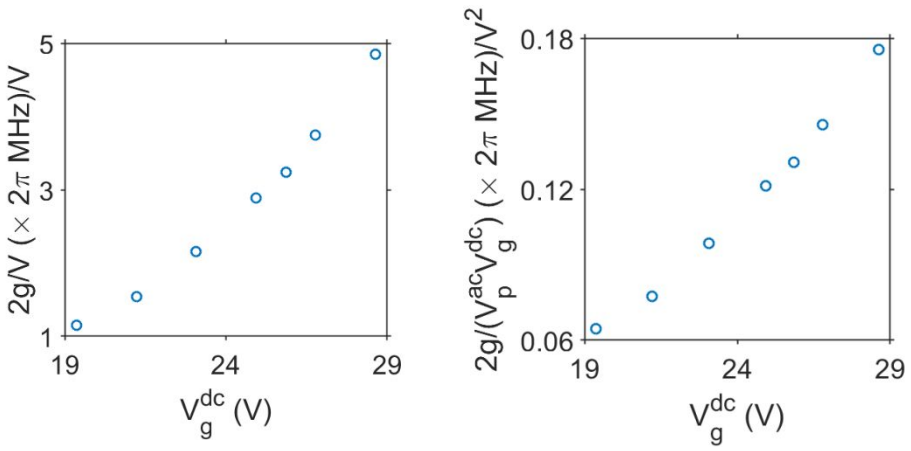

(d) (e)

Figure S5: (a) Splitting of mode 1 with applied pump frequency ω_p at $V_g^{dc} = 26$ V and $V_p^{ac} = 300$ mV. (b) Splitting of mode1 with V_p^{ac} at $\omega_p = 71.5\ (\times 2\pi$ MHz) (Included in the main text for convenience). (c) Coupling rate with pump strength for different V_g^{dc}. Lines are linear fit. (d) Slope of the coupling rate for different gate bias. (e) Coupling rate normalized by V_g^{dc}. Increase in the coupling rate shows that it depends on the tuning of the modes.

VII. Coupling rate for distant modes:

The intermodal coupling constant Λ is given as:

$$\Lambda = \frac{|\alpha_l - \alpha_h| F_p k_c}{2\lambda} \#(S12)$$

Although the relation between spring constant softening and applied gate bias is mode dependent. We attempt to estimate the coupling constant Λ. We know that $\Omega \propto \sqrt{T}$ and force $F \propto (V_g^{dc})^2$ .i.e. $\alpha \propto \frac{\partial T}{\partial F} \sim \frac{\partial \Omega^2}{\partial F}$. Here, we have assumed a linear relation between tension T and V_g^{dc} to have an estimate of the coupling, although the relation is complex.[6] Using the above approximations, equation S12 becomes:

$$\Lambda = \left(\left| \frac{\partial \Omega_l^2}{\partial F} - \frac{\partial \Omega_h^2}{\partial F} \right| \right) \frac{F_p \, k_c}{2\sqrt{\left(\Omega_l \delta\Omega + \frac{\delta\Omega^2}{2} \right)^2 + {k_c}^2}} \#(S13)$$

Where parametric force $F_p \propto V_g^{dc} V_p^{ap}$.

And the coupling rate is given by

$$g = \frac{\Lambda}{2\sqrt{\omega_l \omega_h}}$$

α are estimated from the figure S4 (c) and $k_c = k_{c0} + A\left(V_g^{dc}\right)^2$ where $k_{c0} = 0.25\ (2\pi \times \text{MHz})^2$; and $A = 0.13\ (2\pi \times \text{MHz})^2/\text{V}^2$ are fitting parameters.

REFERENCES:

(1) Prasad, P.; Arora, N.; Naik, A. K. Parametric Amplification in MoS_2 Drum Resonator. *Nanoscale* **2017**, *9* (46), 18299–18304.

(2) Castellanos-Gomez, A.; Buscema, M.; Molenaar, R.; Singh, V.; Janssen, L.; van der Zant, H. S. J.; Steele, G. A. Deterministic Transfer of Two-Dimensional Materials by All-Dry Viscoelastic Stamping. *2D Mater.* **2014**, *1* (1), 011002.

(3) Xu, Y.; Chen, C.; Deshpande, V. V.; Direnno, F. A.; Gondarenko, A.; Heinz, D. B.; Liu, S.; Kim, P.; Hone, J. Radio Frequency Electrical Transduction of Graphene Mechanical Resonators. *Appl. Phys. Lett.* **2010**, *97* (24), 243111.

(4) Okamoto, H.; Gourgout, A.; Chang, C. Y.; Onomitsu, K.; Mahboob, I.; Chang, E. Y.; Yamaguchi, H. Coherent Phonon Manipulation in Coupled Mechanical Resonators. *Nat. Phys.* **2013**, *9* (8), 480–484.

(5) Mahboob, I.; Nishiguchi, K.; Okamoto, H.; Yamaguchi, H. Phonon-Cavity Electromechanics. *Nat. Phys.* **2012**, *8* (5), 387–392.

(6) Eriksson, A. M.; Midtvedt, D.; Croy, A.; Isacsson, A. Frequency Tuning, Nonlinearities and Mode Coupling in Circular Mechanical Graphene Resonators. *Nanotechnology* **2013**, *24* (39), 395702.